

RESEARCH ARTICLE OPEN ACCESS

Advanced Mineral Deposit Mapping via Deep Learning and SVM Integration With Remote Sensing Imaging Data

Nazir Jan¹ | Nasru Minallah¹ | Madiha Sher¹ | Muhammad Wasim² | Shahid Khan³ | Amal Al-Rasheed⁴ | Hazrat Ali⁵ 

¹Department of Computer Systems Engineering, University of Engineering and Technology Peshawar, Peshawar, Pakistan | ²Department of Computer Science, City University of Science and Information Technology Peshawar, Peshawar, Pakistan | ³Department of Electrical and Computer Engineering, COMSATS University Islamabad, Abbottabad Campus, Abbottabad, Pakistan | ⁴Department of Information Systems, College of Computer and Information Sciences, Princess Nourah Bint Abdulrahman University, Riyadh, Saudi Arabia | ⁵Computing Science and Mathematics, University of Stirling, Stirling, UK

Correspondence: Hazrat Ali (hazrat.ali@live.com)

Received: 6 June 2024 | **Revised:** 24 September 2024 | **Accepted:** 14 October 2024

Funding: This work was supported by the Princess Nourah bint Abdulrahman University Researchers Supporting Project number (PNURSP2024R235), Princess Nourah bint Abdulrahman University, Riyadh, Saudi Arabia.

Keywords: carbonated minerals | deep learning | image processing | remote sensing | Sentinel2 | support vector machine

ABSTRACT

Automating mineral delineation and rock type analysis using remote sensing imaging data is a critical application of machine learning. Traditional machine learning methods often struggle with accuracy and precise map generation. This study aims to enhance performance through a refined deep learning model. In this work, we present a deep learning pipeline to map the mineral deposits in the study area. Initially, we apply a deep convolutional neural network (CNN) to a specialized mineral dataset to map mineral deposits within the study area. Subsequently, we build a hybrid model combining deep CNN layers with a support vector machine (SVM). This merger significantly improves classification accuracy from an initial 92.7% to 95.3%. In our approach, CNN layers function as feature extractors while the SVM serves as the classification model. Moreover, we conduct an evaluation of the SVM using polynomial kernels of degrees 3, 6, 9, and 12. The results indicate that the SVM with a degree of 12 achieved the highest classification accuracy, followed by degrees 9, 6, and 3. Experimental results demonstrate the effectiveness of our proposed method for classifying remote sensing imaging data, showcasing its potential for advancing mineral delineation and rock type analysis.

1 | Introduction

One of the vital procedures in the mineral exploration process is to use geological map to analyze and visualize features that are linked with the mineral deposits. These maps include basic data that is relevant to many different fields, such as the study of earthquakes, the development of infrastructure, and the search for groundwater and deep Earth resources [1–4]. Mineral perspective mapping and geological mapping have experienced significant transformations due to the advancements in remote sensing techniques, satellite imagery utilization,

LiDAR data incorporation, enhanced geological understanding, and improved mapping efficiency. Most of the developments in the field can be attributed to the integration of remote sensing data with conventional field observations conducted on the ground [5, 6].

Carbonate species such as CaCO_3 and MgCO_3 play crucial roles in geological studies but are challenging to identify manually, especially in rugged terrains that require extensive labor and resources [7, 8]. The advent of multispectral remote sensing, particularly through platforms like Sentinel-2, has provided a viable

This is an open access article under the terms of the [Creative Commons Attribution](https://creativecommons.org/licenses/by/4.0/) License, which permits use, distribution and reproduction in any medium, provided the original work is properly cited.

© 2024 The Author(s). *Engineering Reports* published by John Wiley & Sons Ltd.

approach for visually detecting carbonates and other geological formations. This has prompted an imperative need to enhance the utilization of satellite imagery for more effective mapping of geological features [9].

The development of image-processing techniques to highlight, distinguish, and categorize geological features has advanced significantly. Although geological mapping utilizing remote sensing data has shown success with a variety of machine learning techniques, including supervised classification techniques, there is still room for improvement in these approaches to enhance the accuracy of classification algorithms and precise perspective map generation [10]. Because machine learning algorithms are data-driven, they can identify patterns in high-dimensional data, which makes them an appropriate choice for handling the increasing databases of remotely collected information in geological mapping applications [11]. Notable machine learning techniques, including dimensionality reduction approaches, k-nearest neighbors (KNN), naive Bayes (NBs), random forests (RFs), support vector machines (SVMs), and multilayer perceptrons (MLP), have been employed to analyze remotely sensed data for geological purposes [12–15].

SVM, recognized as a powerful machine learning approach, has demonstrated effectiveness in tasks such as automated identification of carbonates and supervised classification, providing robust insights into geological features [16, 17]. However, challenges persist in accurately mapping lithological units. Thus, further enhancing SVM capabilities for accurate mapping of rocks, urban areas, vegetation, and water bodies remains a promising avenue. This entails integrating spectral characteristics from diverse data sources, including Sentinel-2 for carbonate and lithological mapping, Landsat 8, Digital Elevation Models (DEMs), and Advanced Land-Observing Satellite/Phased Array Type L-Band Synthetic Aperture Radar (ALOS/PALSAR) data [18, 19].

Convolutional neural networks (CNNs) represent a significant advancement in addressing challenges within geological remote sensing. CNNs are well known for their prowess in image classification, and thus, they offer a promising potential to enhance geological mapping processes. CNNs excel in analyzing remote sensing data, exhibiting the capability to make precise predictions without extensive image preprocessing and effectively handling spatial variations. This resilience to spatial differences renders CNNs highly dependable for processing remote sensing information in geological studies [20, 21]. Recent studies underscore their effectiveness in geological mapping, demonstrating superior performance across diverse applications [22, 23]. Although CNNs have been less explored in mapping potential mineralization zones, their established success in geological mapping and initial surface material classification underscore their potential to transform mineral exploration and mapping methodologies [24].

A novel deep learning approach, integrating CNN and SVM, was proposed for warship sample acquisition, employing transfer learning for validation [25]. Sun et al. utilized a CNN-based method to classify high spectral wetland remote sensing imagery, comparing it with Texture-Spectrum SVM (TSPSVM) and Spectral Feature SVM (SP-SVM) approaches [26]. Han et al. [27], used a pre-trained AlexNet to classify remote-sensing image scenes.

Additionally, the authors in [28, 29] introduced an innovative ship target recognition method that integrates feature aggregation with transfer learning from SAR images. Their approach involved crafting test datasets with diverse resolutions, sizes, sea conditions, and sensor types, highlighting the pivotal role of CNNs in feature extraction and classifier development tailored to various forms of remote-sensing images. However, despite the advancements achieved in previous research, we must confront and address persistent challenges and limitations [30, 31]. Conventional methods in machine learning such as NBs, RFs, and KNN often struggle to achieve high accuracy and precise map generation in geological mapping [32]. These methods have inherent limitations when dealing with high-dimensional and complex remote sensing data. In addition, the manual identification of carbonate species and other geological formations is labor-intensive and resource-consuming, particularly in complex environments, requiring the development of automated techniques that improve accuracy and efficiency. While SVM-based approaches have been promising in the classification of minerals, their performances can be further improved when integrated with deep learning models like CNNs [26]. Likewise, CNNs excel in feature extraction but can benefit from the classification robustness of SVMs. Hence, it is pertinent to explore the potential of machine learning and deep learning hybrid models in remote sensing data. One key challenge in developing a hybrid model is to achieve model generalization so that the trained model can adapt to data from diverse geological terrains [33]. This study addresses these challenges through an in-depth analysis of various polynomial kernel degrees in SVM to identify the optimal configuration and evaluate the trained model using unseen test data from a different geological location. By highlighting these shortcomings and addressing them with our hybrid model, we developed a model to demonstrate how our approach advances mineral mapping methodologies, contributing significantly to the field of geological remote sensing.

In this study, we build a hybrid model combining CNN and SVM and use it for mineral mapping. The ability of SVMs with higher-degree polynomial kernels to represent complex, non-linear connections in high-dimensional feature spaces allows them to work better than other machine learning algorithms on the task of classification of minerals. To convert the initial feature space into a higher-dimensional space, the SVM can be effectively used with a higher-degree polynomial kernel, allowing SVMs to identify nonlinear correlations in mineral data that a linear kernel would overlook. We then explore the potential of the hybrid model and the effect of varying SVM polynomial degrees on the classification performance. By systematically investigating these modifications, we aim to enhance the efficacy of the hybrid model, providing valuable insights to optimize mineral mapping techniques for remote sensing data. Our results demonstrate a notable improvement in model accuracy and the potential for enhanced map generation.

2 | Background

This section highlights the applications of machine learning and deep learning methods in mineral exploration.

Geological mapping has been revolutionized by the integration of remote sensing information and advanced machine learning methods. This has allowed for more efficient and cost-effective mapping of lithological units and geological formations [34–36]. The use of remote sensing multispectral imagery, particularly with advancements in sensors available via platforms like Sentinel-2, has enhanced the visual examination of geological features [37, 38]. In recent years, the domain of mineral exploration has experienced notable progress. The incorporation of machine learning methods in remote sensing data analysis has emerged as a pivotal factor in augmenting the capabilities of deep neural models [39–41]. Study in [42] has developed a compressed sensing-based method for 3D rain field tomographic reconstruction using simulated satellite signals, enhancing meteorological data analysis for better weather prediction. Additionally, another study conducted in [43], introduced the Modality Fusion Vision Transformer, which significantly improved collaborative classification of hyperspectral and LiDAR data.

2.1 | Support Vector Machine

SVM represents a significant leap forward in contemporary machine learning [44, 45]. A standout characteristic of SVM lies in its utilization of kernel functions. Constructing a linear boundary within a high-dimensional space, the kernel function adeptly handles nonlinear problems within the input feature vector set. Simultaneously, it transforms non-convex optimization into convex optimization, effectively overcoming challenges associated with local minima and facilitating global optimization in classification. The essence of SVM lies in the determination of an optimal classification hyperplane, expressed as $\omega^T x + b = 0$, where ω is the weight vector, x is the input feature vector, and b is the bias term. To achieve this, the SVM formulation incorporates a constraint:

$$[y(\omega^T x + b) \geq 1 - \xi]$$

where y represents the target output, and ξ is a slack variable accounting for deviations from the optimal classification. The subsequent expression for the optimal classification hyperplane is:

$$\min \left(\frac{1}{2} \|\omega\|^2 + C \sum_{i=1}^N \xi_i \right)$$

Note that C is the penalty coefficient. The objective of using C is to regulate the wide-margin classification objectives while also keeping the misclassification minimum. SVM maps the input data into a higher dimensional space using the kernel function. This, in turn, enables the hyper-plane between samples that are otherwise highly non-linearly separable. We use the Radial Basis Function (RBF) as the kernel function K , as shown in Equation (1):

$$K(x_i, x_j) = \exp \left(-\frac{\|x_i - x_j\|^2}{2\sigma^2} \right) \quad (1)$$

Here, the parameter σ determines the kernel width that in turns impacts the decision boundary smoothness. For complex data with non-linear separation, the RBF kernel is a common choice for SVM classifiers.

2.2 | CNNs in Mineral Data Processing

Deep learning models, including CNNs have demonstrated significant potential in computer vision applications such as image classification and object detection [46, 47]. In the domain of mineral exploration in remote sensing images, the potential of CNNs has been explored to analyze geological and remote sensing data for identifying mineral deposits and predicting their characteristics [48].

Typically, CNN architecture comprises multiple convolution and pooling layers. In the convolutional layers, kernel functions are multiplied and added with the input features to extract complex feature maps. Then, by using subsampling layers, these traits are expanded into higher levels, improving their resilience and abstraction.

Consider a d -dimensional input data, that is, $x \in \mathbb{R}^d$. For a given input x , the output of any convolution layer l can be expressed by Equation (2) as:

$$h_{ij}^l = f \left(\sum_{i,j}^{N_l} (k_{ij}^l * x) + b_j^l \right) \quad (2)$$

Here, $f(\cdot)$ is an activation function, which could be sigmoid, Rectified Linear Unit (ReLU), or hyperbolic tangent. The symbol $*$ denotes the convolution operation, and N_l denotes the number of input feature maps. The term k_{ij}^l represents the kernel operating on the i th feature map of layer $l-1$ to produce the j th feature map of layer l , and b_j^l is the bias for the j th feature map of layer l . If $l=1$, then $h_x^1 = x$ is the input layer. The convolution layers generate features that are then directed to the pooling layer. Common pooling functions, such as average pooling, sub-sampling, and max-pooling, are employed in this stage. The outcome of sub-sampling is described in Equation (3):

$$S_j^l = g \left(\gamma \cdot \frac{1}{n \times n} \sum_{i,j} (h_{ij}^{l-1}) + b_j^l \right) \quad (3)$$

Here, the average of an $n \times n$ patch of the previous layer's j th feature map is taken, multiplied by a trainable scalar γ , and added to a bias b_j^l , passing through a non-linear function $g(\cdot)$. Convolution layers are typically followed by pooling layers to minimize computational complexity and spatial size. This lessens the possibility of overfitting and improves feature robustness as well. We have utilized the max pooling activation function in the study.

2.3 | Hybrid Models for Minerals Data Processing

Ensemble models refer to the integration of multiple machine learning algorithms or models to improve the overall performance [49]. In the context of mineral exploration, this technique has been used to combine the strengths of various approaches, including SVMs and deep neural networks, thus, achieving more accurate and robust predictions. The merger of models can help overcome the limitations of individual algorithms and enhance the overall predictive power [50, 51].

Traditional classification methods for remote sensing imagery often rely on conventional feature extraction and selection techniques. However, these approaches can exhibit limitations in pertinence, accuracy, and computational efficiency when applied to complex remote sensing images [26]. Recent advancements in machine learning algorithms and spatial modeling techniques have significantly advanced the predictive modeling of mineral prospects in specific regions, such as the southern Jiangxi province of China. These studies have employed a range of methods including artificial neural networks (ANNs), CNN, SVM, and RFs [39]. In another study, Wan et al. [52] proposed a CNN-SVM-based multi-scale spectral-spatial remote sensing approach to classify coral reef environments on Zhaoshu Island and Zhong Island in China. Additionally, Hajaj et al. [53] utilized SVM, 1D-CNN, RF, and KNN for lithological mapping in complex hydrothermal areas. These contributions are valuable for exploration geologists seeking suitable techniques for precise mineral mapping in diverse metallogenic provinces. Further notable contributions in remote sensing imagery analysis are reported in [54, 55].

2.4 | Recently Used Methods for Mineral Exploration

In a study by Eskandari et al. [56], the existing gaps among UAV photogrammetry, satellite remote sensing, and field data were bridged in order to better define the criteria for locating chromite-bearing mineralized zones. The study exercised three steps toward achieving the goals by first, employing satellite remote sensing to identify the most promising lithological units for chromite mineralization. Second, the ultra-resolution RGB Minerals orthomosaic data was obtained by unmanned aerial vehicle (UAV) mapping which was then utilized to manually distinguish geological units and structures. In the final step, the SVM was used to categorize lithological units and peridotites with varying serpentinization levels. Another recent study by Iqbal et al. [57], analyzed the existing applications of Artificial Intelligence (AI) and machine learning in mineral exploration and assessed their potential and limitations. It explored the potential benefits and drawbacks of incorporating AI and machine learning approaches into this industry while making important recommendations for future research and development to improve the use of AI and ML in mineral exploration. The noteworthy of them are; the integration of machine learning and deep learning hybrid approaches to witness significant accuracy, enhancing the AI-based models' precision by using other data sources, such as geological, geochemical, and remote sensing data, and the involvement of easily understandable and comprehensible AI methods like rule-based models and decision trees in mineral exploration to better understand the geological knowledge in contextual data. In [58], the authors provided a method for determining the most optimum and efficient machine learning strategy for lithological mapping, utilizing advanced space-borne thermal emission and reflection radiometer (ASTER) remote sensing data. This study compared traditional machine algorithms (RF and SVM) to novel ensemble machine learning techniques (gradient boosting, eXtreme Gradient Boosting, and deep learning ANN) for spatial modeling of lithological units. Another study in [59] provided a course for the field's development by introducing some of the most recent deep learning approaches that have

not previously been used for remote sensing, such as graph deep learning methods, Bayesian deep learning, variational autoencoders, and transformer recurrent neural networks. In [19], the integration of three separate multispectral remote-sensing data sets, namely Landsat 8 operational land imager (OLI), ASTER, and Sentinel-2, was used to obtain a detailed classified map of the study region. Traditional machine learning methods, like SVMs, and MLP as well as deep learning methods, that is, CNN, were applied to the available satellite data.

3 | Methodology

3.1 | Geology of Study Area and Image Acquisition

The Mardan and Buner region of Khyber Pakhtunkhwa (KP) Pakistan is well known for having abundant mineral deposits. Massive amounts of marble, soapstone, granite, limestone, iron ores, and other valuable minerals have been identified through a survey conducted by the KP Government Minerals Department, as documented on the department's portal.ⁱ These resources have been made available for open leasing to several businesses for extraction and processing. Substantial carbonated mineral deposits are available there, which can be seen using the coordinates 32° 12' 11" N and 72° 20' 07" E, as well as in the surrounding area. While visiting the location, a survey team from the Lab of the National Centre for Big Data and Cloud Computing (NCBC), University of Engineering and Technology Peshawar, collected field samples and the research area's coordinates through the Global Positioning System (GPS). Following this, remote sensing data of the intended study region (Sentinel-2) was downloaded from The United States Geological Survey (USGS) Earth Explorer,ⁱⁱ as shown in Figure 1.

To prevent biases in the final results, the data sets used for training and testing were gathered from separate and independent geological sites during the data acquisition process. Two large areas were chosen to gather training data: the Shabbaz Garhi region in Rustam (Mardan district) and the Pathorra region (Buner district) mines. Test data, used for validation, were collected from the Bagh mine, which served as an additional independent location. There is adequate data available at these places spanning a wide geographic area dispersed over miles, providing sufficient coverage for the study.

3.2 | Preprocessing

During the experimentation, remote sensing granules underwent a variety of processes and treatments, as shown in Figure 2 to transform them into useful, informative maps. In Figure 2, the left side represents the processing steps responsible for preparing the refined dataset polygons from the downloaded remote sensing imagery of the study area location. Specifically, it comprises three modules that provide information related to; (a) the source of the remote sensing data for the study area, (b) the preprocessing steps employed to prepare the remote sensing data, and (c) the extraction and normalization of mineral's related particular dataset points from the imagery. The right side of Figure 2 represents the steps that are adapted

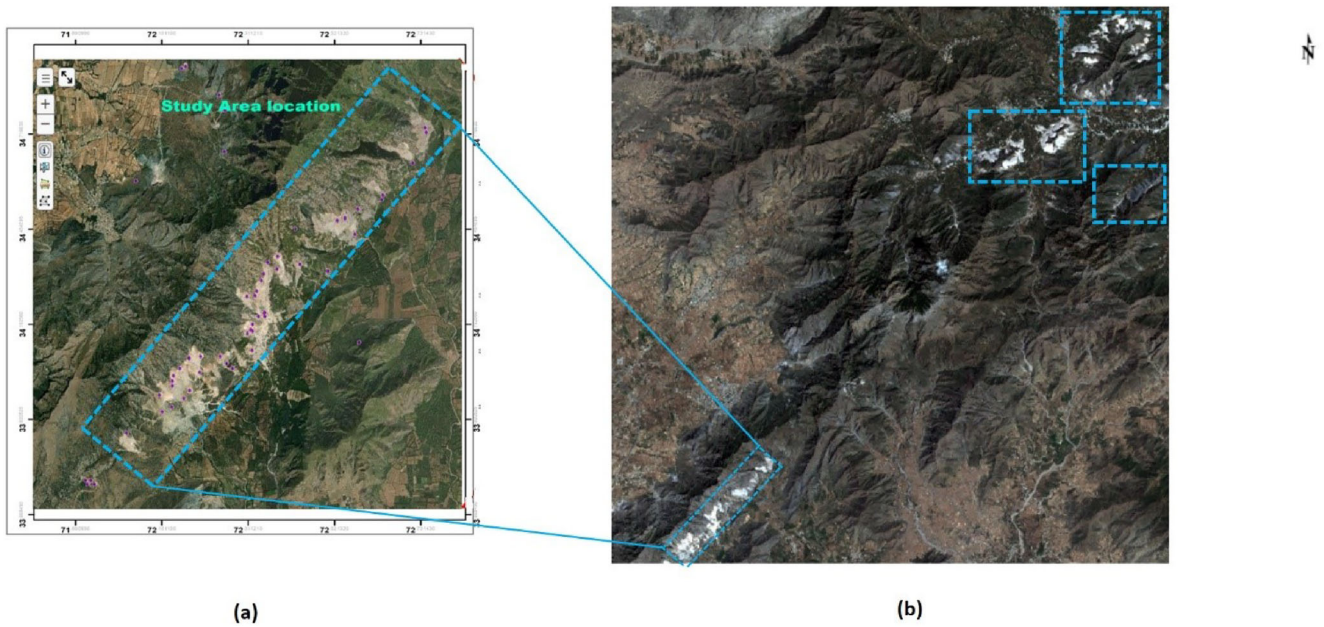


FIGURE 1 | (a) Mineral polygons available in the intended study area. (b) Sentinel-2 imagery of the intended study area.

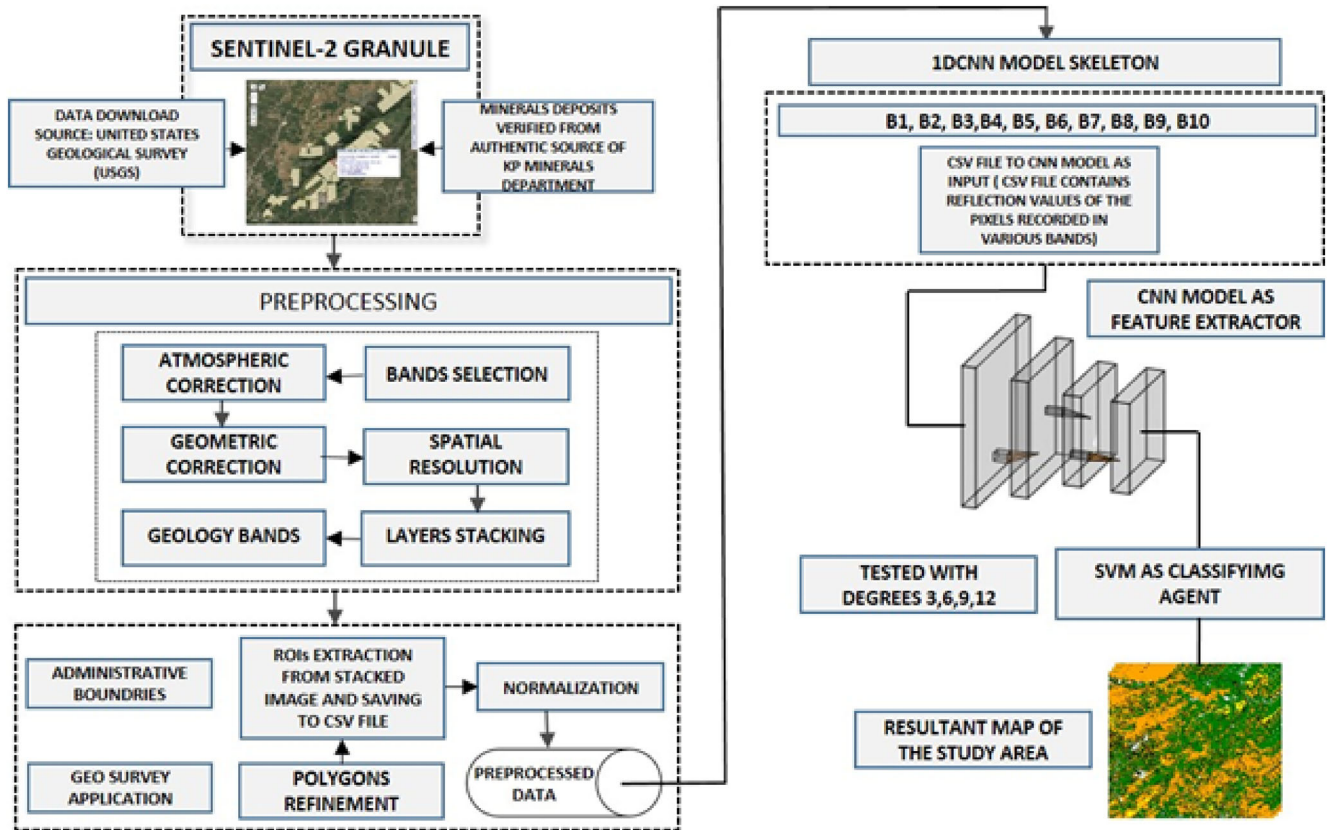


FIGURE 2 | The workflow of the study. The left side represents the data acquisition, various preprocessing, and data extraction steps. The right side represents the 1-dimensional data preparation, model training for feature extraction and classification, and visualization steps of the study area map.

for: (a) generating the 1-dimensional CSV file containing the reflectance values of minerals and other classes as collected from the study area, (b) the proposed model training and classification workflow using various parameters, and (c) the final visualization of the resulting study area map which highlights

the potential zones of interest. To accomplish goals like data refinement, data dimensionality reduction, and several other tasks, the treatments involve preprocessing, image processing, and classification processes. The following steps are covered in detail:

Preprocessing procedures are essential for transforming raw remote sensing data into usable reflectance images, enabling accurate analysis and interpretation. Two primary objectives were pursued in this process: noise removal and conversion of radiance data to reflectance images. Initially, the raw data underwent cleaning to eliminate atmospheric noise artifacts. Subsequently, the radiance data captured by the sensors was converted into reflectance images. This conversion is crucial as it standardizes the data and facilitates spectrum mapping and object identification. Each pixel in remote sensing imagery is represented by a Digital Number (DN), which aggregates information from various ground features within the pixel's footprint. To derive meaningful reflectance values, these DN readings are first transformed into surface radiance images through Radiometric Calibration (RC). Subsequently, the radiance images are converted into Absolute Reflectance (AR) images using the method found in Equation (4).

$$\rho = \frac{\pi \cdot L_s}{d^2 \cdot ESUN_s \cdot \cos(\theta_s)} \quad (4)$$

ρ , unitless planetary reflectance; L_s , spectral radiance at the sensor's aperture; d , Earth–Sun distance in astronomical units; $ESUN_s$, mean solar exoatmospheric irradiance;

θ_s , Solar zenith angle.

The resulting absolute reflectance (AR) images represent data that has undergone both geometric and atmospheric corrections, ensuring suitability for subsequent tasks such as feature identification and classification. These adjustments are crucial for preparing imagery optimally for accurate scientific analysis. This is worth mentioning that geometric correction is an important preprocessing method that aligns RS imagery in correct way in the geographic space. It adjusts the images to a standard coordinate system and maps the projection environment to carry accurate spatial information of pixels within the imagery. Geometric correction is responsible for locating the control points within the imagery that coincide with specific surface points such as construction sites, roads, vegetation, and other objects. Using mathematical transformations on the map axis points to align the control points with their known locations, the resulting imagery turns into an accurate representation of the study area location. Most of these correction procedures are typically applied to Level 1 (L1) data as hyperspectral data is commonly delivered in L1 format, necessitating manual corrections of this nature. However, for the proposed study project utilizing Sentinel-2 multispectral granules, the data was obtained in Level 2 (L2) format from the USGS Earth Explorer. Granules in L2 format have already undergone geometric and atmospheric adjustments by the data provider, eliminating the need for additional processing steps. Despite the preprocessing done by the data provider, it remains essential to provide readers with a basic understanding of the associated terminology for clarity and comprehension.

To improve visual quality and facilitate detailed analysis, selected bands from Sentinel-2 imagery were stacked and resampled to achieve a spatial resolution of 10 m. The resampling method converts an image of low spatial resolution into a higher resolution which provides more insight into the surface area. We employed the nearest neighbor resampling algorithm to convert Sentinel-2

low spatial resolution bands of 20 m into 10-m bands. The stacked imagery consisted of all the chosen bands in a layered fashion. Layer stacking is important to generate imagery that holds the reflectance of all the selected bands in a layered fashion making it suitable for classification task. We employed a layer-stacking algorithm to get the desired stacked imagery. When viewing remote sensing data, various false color combinations can be employed to highlight specific features and characteristics. In this study, bands 7, 5, and 3 of the Sentinel-2 imagery were assigned to the red, green, and blue channels, respectively. This combination is often utilized to enhance the visualization of natural exposures of minerals and geological structures within the study region. Lastly, the data were standardized to make it ready for the subsequent application. A common preprocessing step in data analysis is normalization, which involves modifying the data to have a mean (average) of 0 and a standard deviation of 1. By doing this, the original data's scale will no longer influence the analysis and the data will be more comparable. After being recovered from the satellites imagery, the data for the current study is normalized. Standardization is carried out to guarantee that every variable (band reflection value) is given the same weight in the analysis, getting rid of any potential bias brought on by variations in the data's magnitude.

3.3 | 1-Dimensional Data Vectors Preparation

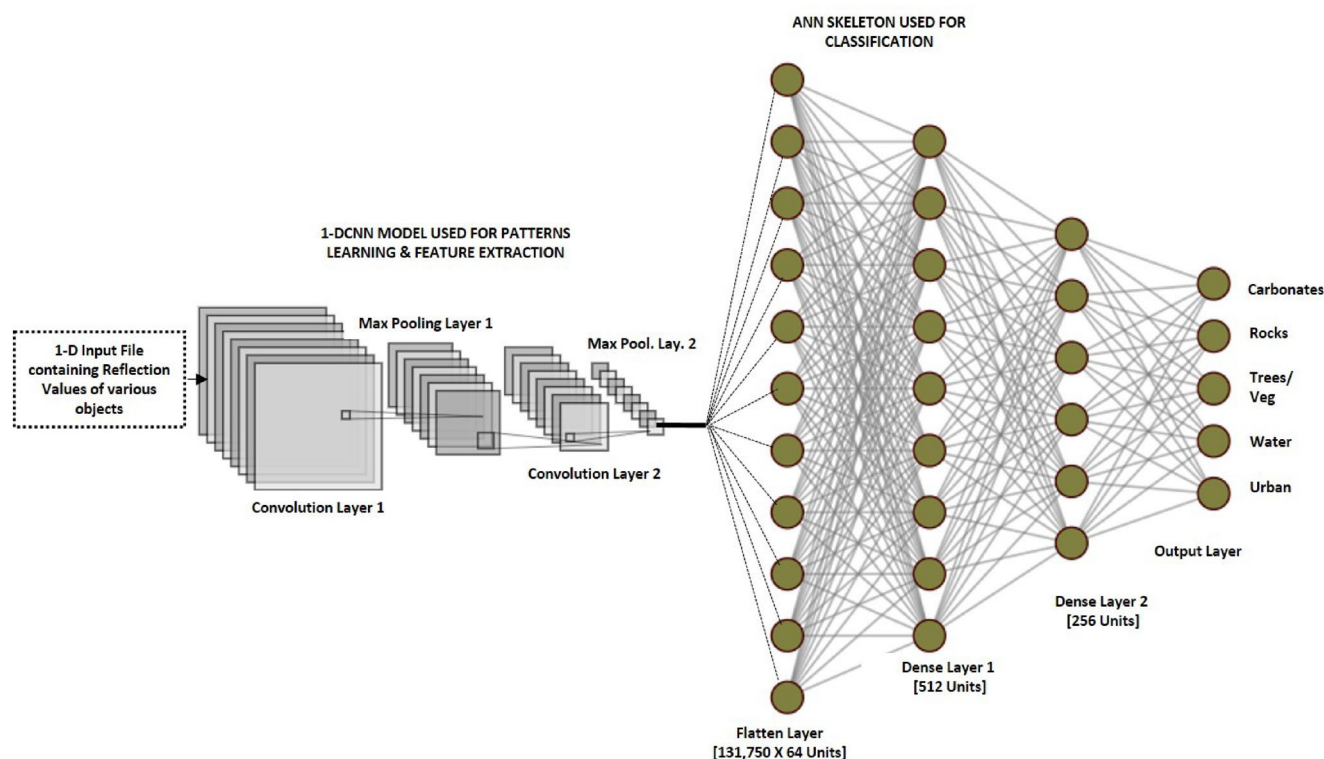
Shapefiles containing training polygons representing different class members within the study area were utilized to create clean Region of Interest (ROI) masks for each class. These ROIs were manually defined to accurately capture specific features of interest. Pixel reflectance values corresponding to the ROIs were extracted and recorded into CSV files. These CSV files serve as essential input data for training deep learning and machine learning models, providing the necessary feature vectors for classification tasks. Table 1 summarizes the total number of polygons and associated pixels for each class member within the training and test sets, offering insights into the dataset's composition and distribution, as reported in [60].

We saved the shape files for the training polygons we made of the different class members from the study area. The imported shape files were used to manually create clean ROIs for every class member, and the pixel reflectance values were recorded and stored in CSV files for use as input in deep learning and machine learning models. Table 1 displays the total number of polygons and pixels for each class member in the training-test set.

In contrast to two-dimensional image or time series data, our dataset consists of one-dimensional reflectance values measured by satellite sensors, which are stored in CSV files. We have designed a 1-D CNN-SVM model tailored to the characteristics of this dataset for testing and classification purposes. A single ROI may contain one or more pixels, depending on the size of the ROI that is produced. A pixel resolution of 10×10 is associated with Sentinel-2 data with a spatial resolution of 10 m. Pixel size refers to the area that Sentinel-2 sensors cover in a single pixel when gathering a surface image. To prepare for model training and evaluation, the dataset was split into training and test sets using various ratios, including 80:20, 70:30, and 60:40 for training-test splits. Improved performance was observed with a 70:30 ratio,

TABLE 1 | Training and test sets data preparation details, data reported from [60].

Class members	Training polygons	Test polygons	Number of pixels
Urban	327	112	23,502
Trees/vegetation	410	133	24,823
Water	67	23	25,027
Carbonates	319	129	31,253
Rocks	378	123	27,145
	Total = 1501	Total = 520	—
	Grant total = 2021		Total Pixels = 131,750

**FIGURE 3** | 1-D CNN-ANN architecture.

indicating a balanced distribution between training and test data. The selected model was trained using 70 epochs to ensure sufficient learning and convergence. It was crucial to maintain the independence of training and test datasets to avoid introducing biases in the evaluation and validation of model performance.

3.4 | The Proposed Model: 1-D CNN-SVM Merger

The study focused on evaluating a novel hybrid model architecture combining 1-Dimensional CNN (1-D CNN) layers with an SVM, as illustrated in the methodology diagram in Figure 2. Initially, a neural network model was constructed using convolutional layers followed by max-pooling layers (1-D CNN). This architecture was designed to extract feature maps from the one-dimensional CSV files during the feature engineering process. The extracted feature maps were subsequently fed into dense layers of an ANN to perform classification across different

categories. The combined 1-D CNN-ANN architecture is depicted in Figure 3. The 1-D CNN-ANN model achieved ~93% accuracy when trained and tested on the dataset. Various configurations of convolutional layers and max pooling layers were explored, with the most effective setup involving two convolutional layers and two max pooling layers.

Subsequently, the proposed model integrated the 1-D CNN architecture with SVM to assess whether further improvements in classification accuracy could be achieved. In this hybrid model, the convolutional layers were responsible for feature extraction and dimensionality reduction through filter operations, while the SVM model handled the classification tasks across multiple categories. The integration of SVM with the 1-D CNN architecture aimed to leverage the strengths of both approaches, enhancing the model's overall performance in classifying the carbonated data accurately. In all our implementations, we employed ReLU as the activation function. CNN is a multilayered design that receives its initial input data from the input layer. The

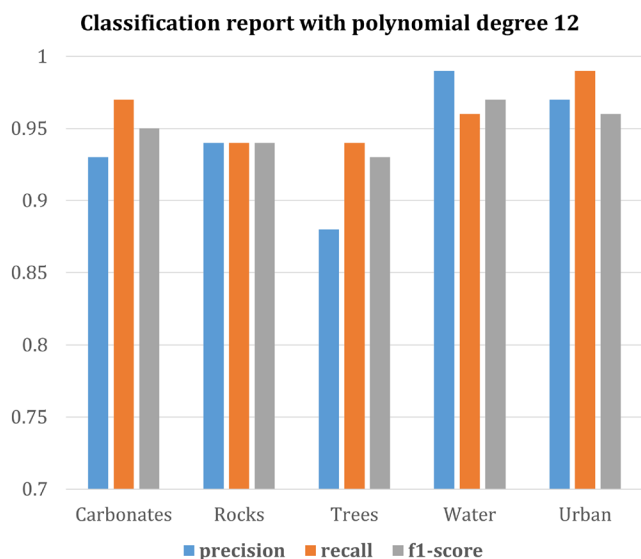


FIGURE 4 | 1-D CNN-SVM-polynomial degree 12 classification report.

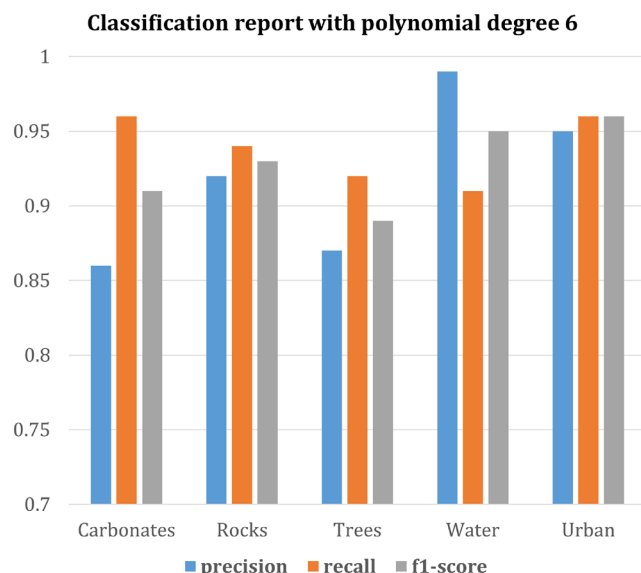


FIGURE 6 | 1-D CNN-SVM polynomial degree 6 classification report.

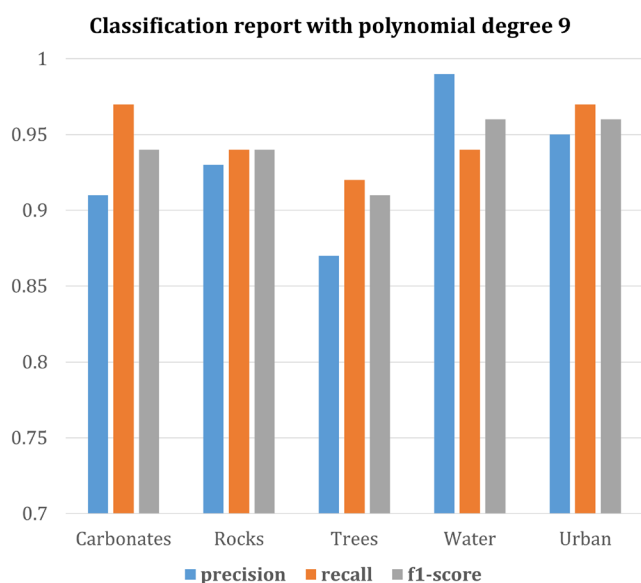


FIGURE 5 | 1-D CNN-SVM polynomial degree 9 classification report.

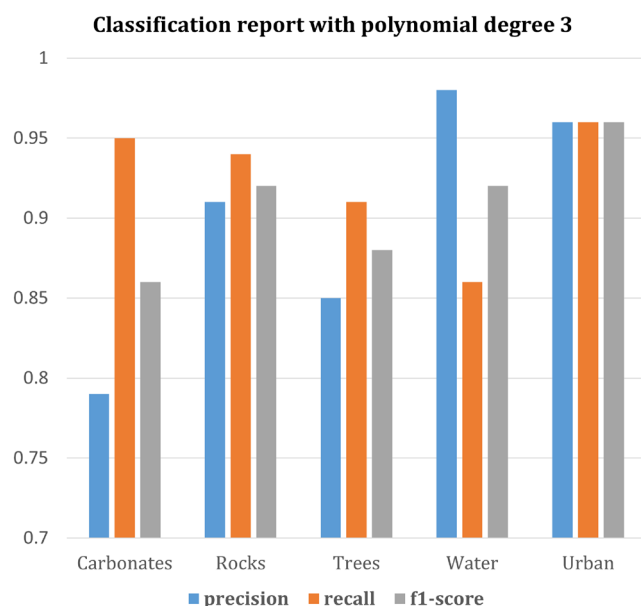


FIGURE 7 | 1-D CNN-SVM polynomial degree 3 classification report.

design skeleton used in this study is based on one-dimensional (1D) spectral reflectance data collected across many bands. It gets the 1D spectral reflectance data as an input from the input layer which passes the data to convolutional layers. Being the core part of the architecture, the CNN layers process the 1D spectral reflectance data with adaptable filters, known as kernels. The model obtained optimum results by using a couple of CNN layers with the first containing 32 filters that convolve over the input data. These filters recognize features and patterns, spectral properties, and absorption features in the reflectance data. Following this, the second convolutional layer with 64 filters is applied which seeks to extract more complicated spectral information by merging and expanding the patterns observed in the previous layer. This hierarchical feature extraction approach improves the model's ability to identify subtle spectral properties required for accurate mineral classification. The pooling layer is

located in the midst of the subsequent convolutional layers and is mostly used for picking features and information filtering. Pooling layers are often introduced at regular intervals between convolutional layers. The two most common pooling strategies are Max Pooling, which selects the maximum value of the sliding window, and Average Pooling which selects the sliding window's average value. We have utilized two Max pooling layers in the designated CNN architecture (Figures 4–7 and Tables 2–5).

In our experiments, we evaluated the performance of SVM with different degrees of polynomials, that is, degrees 3, 6, 9, and 12. In each experiment, we trained and tested the hybrid model independently for each value of the polynomial degree. Thus, a systematic assessment is performed to analyze the impact of changing the polynomial degree on the classification accuracy.

TABLE 2 | Confusion matrix for polynomial degree 12.

Model		Carbonates	Rocks	Trees	Water	Urban
Hybrid model	Carbonates	97.28	1.4	0	1.3	0.12
	Rocks	1.12	94.46	4.07	0.18	0.16
	Trees	0	6.42	92.92	0.24	0.42
	Water	1.79	1.5	0.49	95.21	1.01
	Urban	0.05	1.22	0.65	0.57	97.5

TABLE 3 | Confusion matrix for polynomial degree 9.

Model		Carbonates	Rocks	Trees	Water	Urban
Hybrid model	Carbonates	96.82	1.53	0	1.61	0.04
	Rocks	0.9	94.07	4.49	0.35	0.19
	Trees	0	7.17	92.21	0.17	0.45
	Water	2.9	1.71	0.56	93.85	0.99
	Urban	0.05	1.25	0.79	0.71	97.21

TABLE 4 | Confusion matrix for polynomial degree 6.

Model		Carbonates	Rocks	Trees	Water	Urban
Hybrid model	Carbonates	96.27	1.82	0	1.87	0.04
	Rocks	0.73	93.98	4.41	0.62	0.26
	Trees	0	7.69	91.76	0.14	0.4
	Water	24.96	2.19	0.76	91.24	0.85
	Urban	0	1.55	0.9	0.81	96.74

TABLE 5 | Confusion matrix for polynomial degree 3.

Model		Carbonates	Rocks	Trees	Water	Urban
Hybrid model	Carbonates	95.23	2.17	0	2.38	0.21
	Rocks	0.46	93.83	4.32	1.1	0.29
	Trees	0	8.73	90.8	0.12	0.35
	Water	8.62	3.5	1.25	85.96	0.66
	Urban	0.08	2.06	1.25	1.06	95.55

TABLE 6 | Confusion matrix for ANN-softmax.

Model		Carbonates	Rocks	Trees	Water	Urban
ANN (dense layers)	Carbonates	3391	81	0	4	0
	Rocks	3	8166	319	0	70
	Trees	0	712	3502	0	24
	Water	9	0	0	7162	23
	Urban	4	49	12	50	3571

TABLE 7 | Confusion matrix for 1-D CNN-RF architecture.

Model		Carbonates	Rocks	Trees	Water	Urban
Hybrid Model	Carbonates	98.65	2.41	0	1.1	0.11
	Rocks	1.08	93.01	5.4	1.54	1
	Trees	0	3.82	93.4	0.22	1
	Water	0.23	0.65	0.85	94.92	0.22
	Urban	0.04	0.11	0.35	2.22	97.67

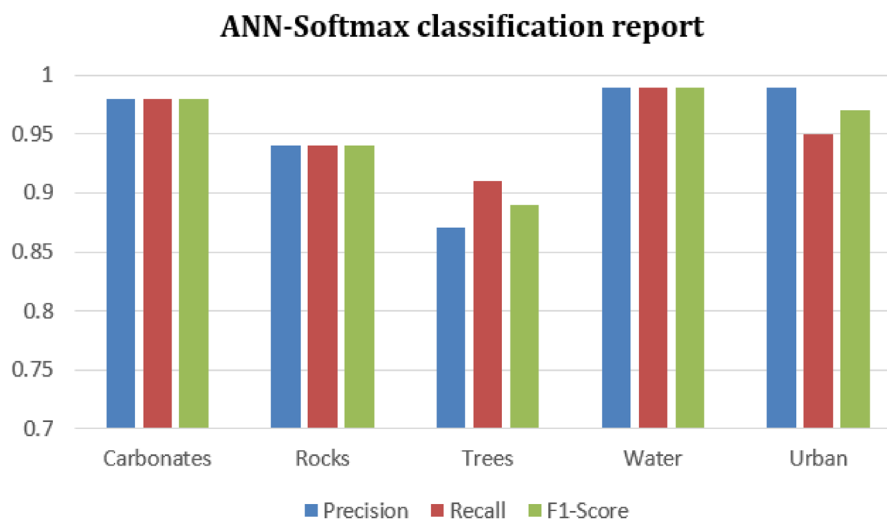


FIGURE 8 | ANN-softmax classification report.

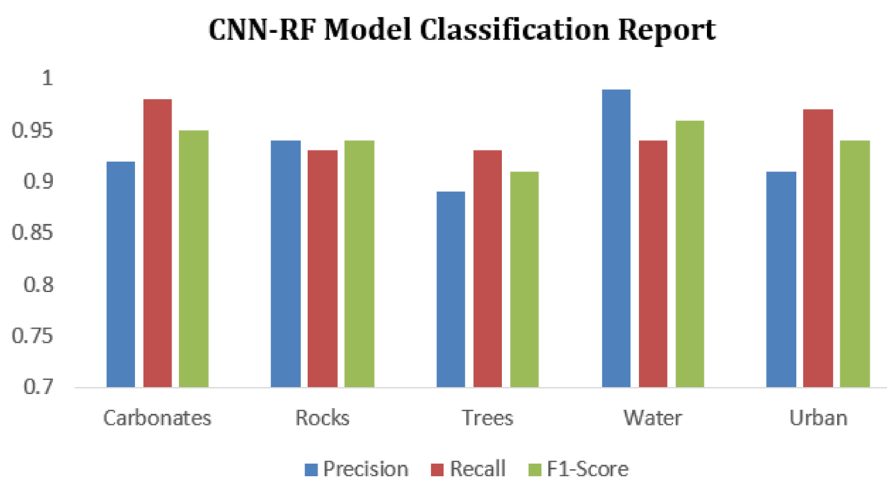


FIGURE 9 | 1-D CNN-RF classification report.

In this study, apart from implementing and evaluating the proposed model, we have also investigated other models on a locally generated mineral dataset of a 1-dimensional format specifically designed for the models under study. The study mainly focuses on investigating the performance of DL-ML hybrid approaches, especially the proposed 1-D CNN-SVM merger on mineral's study, yet providing the detailed outcomes of baselines like ANN-Softmax, CNNs, and a 1-D CNN-RF hybrid model on the same dataset for the purpose of comparison and reader understandability detailed in Section 3.5. More recent baseline deep learning models like LSTM and RNNs [61, 62] are suitable for handling multi-dimensional data like grids and time series data for crop studies, environmental monitoring, and glaciers analysis which need temporal data for detecting changes over the years.

3.5 | Comparison With ANN-Softmax and 1-D CNN-RF Hybrid Models

During the experimentation, we evaluated the performance of the additional models on the same dataset, that is, a dense layered neural network architecture combined with Softmax layer

(ANN-Softmax) and a 1-Dimensional CNN-Random Forest (1-D CNN-RF) hybrid model. In the former, the data enters the dense layers using its input layer which is designed to handle the satellite image's spectrum information. Each dense layer consists of interconnected neurons, representing pixels from the satellite data, and its values encode the pixel's intensity or spectral properties. Dense layers, also called fully connected layers, perform the feature extraction. We experimented with various number of dense layers combined with Softmax layer to classify mineral's and rock data into various classes. However, better results were achieved when we used two dense layers followed by a Softmax layer that performed the final classification of the input data. Softmax layer turns the raw output from the preceding layers into a probability distribution across classes. Each neuron in this layer represents the probability that the input belongs to a particular class. In the 1-D CNN-RF hybrid model combining the CNN with a random forest model, we used the same CNN architecture with similar parameters and input dataset, as we used in our proposed 1-D CNN-SVM model. CNN was used to extract features from the input data whereas the random forest part was used to classify the data in various classes. RFs method develops a combination of decision trees based on the extracted patterns and features. Every

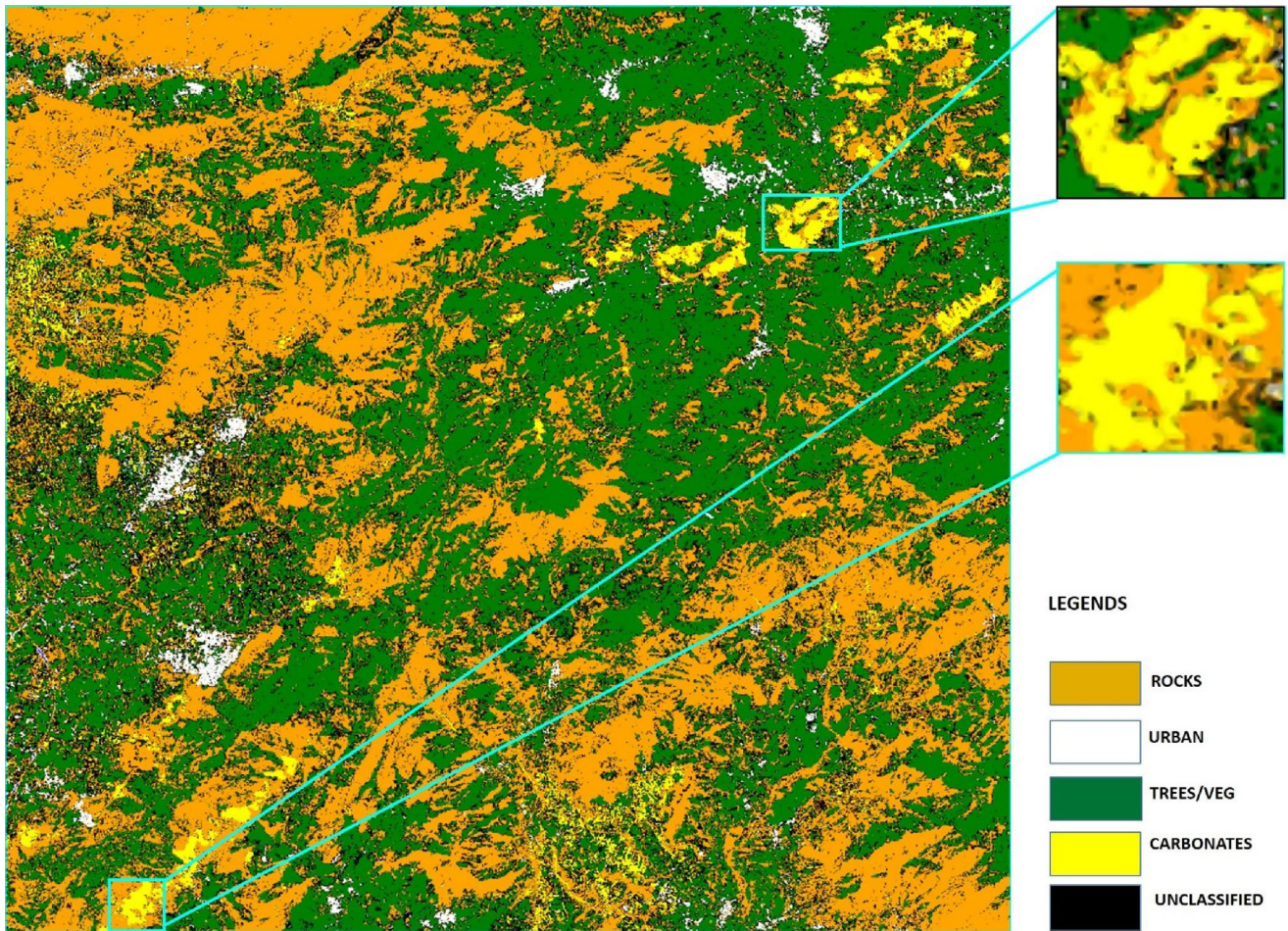


FIGURE 10 | The classified resultant map (Sentinel-2) of the intended study region yielded by the proposed model with different legends showing the texture of the study area.

single tree makes prediction of its own based on the input data. The overall classification decision was established averaging the individual trees prediction. The performance evaluation of both the models is presented in the results section. Their confusion matrices and complete classification reports in graphical representation are presented in Tables 6 and 7 and Figures 8 and 9, respectively.

4 | Results and Discussion

In this section, we present the results obtained for delineating mineral zones and report the improvements in classification performance as obtained by combining SVM with the CNN model, thus, assessing the effectiveness of the hybrid model.

The SVM algorithm was evaluated using various degrees of polynomial kernels to classify the data into multiple classes. Here, we present the detailed results of these experiments, highlighting the performance achieved with each polynomial degree. Notably, the model with a polynomial degree of 12 consistently demonstrated superior results. This optimal setting significantly enhanced the performance of the convolutional layers, leading to improved accuracy and effectiveness in classifying the dataset. Figures 4–7 and Tables 2–5 illustrate detailed experimentation

results and classification reports of the proposed 1-D CNN-SVM model. Additionally, the resultant classified map of the study area generated by the model with polynomial degree 12 is shown in Figure 10.

The findings reveal several important insights supported by detailed classification reports and statistical analyses. Specifically, the SVM model's ability to capture complex data correlations improves with higher polynomial degrees, allowing for better adaptation to intricate patterns within the dataset. This capability is particularly crucial when dealing with the complex, nonlinear interactions observed in mineral zones. A polynomial degree of 12 exhibits superior performance by accurately capturing subtle features and nuances in the training data that might be missed by lower-degree polynomials. This level of complexity strikes an optimal balance between model variance and bias, resulting in enhanced overall accuracy.

The model's accuracy and Kappa score were analyzed for each degree, demonstrating distinct performance characteristics. Specifically, at a polynomial degree of 12, the model achieves the highest accuracy of 95.26% and a Kappa score of 0.936. As the degree decreases to 9 and 6, accuracy and Kappa scores decline accordingly. For example, degree 9 polynomial yielded an accuracy of 94.46% and a Kappa score of 0.925%, and degree 6

polynomial achieved an accuracy of 93.26% and a Kappa score of 0.9095%. The outcomes from the other tested models stood runner up yielding better accuracies and Kappa scores. The ANN-Softmax model generated 93.4% accuracy and a Kappa score of 0.927 whereas the 1-D CNN-RF merger obtained 94.01% accuracy and a Kappa score of 0.931. These values show greater promise of DL-ML hybrid approaches for mineral and rock study by utilizing multispectral sensors' bands. The performance of dense layers and convolutional layers in mineral's classification sees significant improvement when merged with conventional machine learning models, especially RFs and SVMs. Furthermore, the resultant classified map effectively distinguishes mineralization zones with greater clarity and detail. Mineral zones within the Pathorra (Buner district) and Rustam were accurately mapped and cross-verified during site visits by team members from the National Center for Big Data and Cloud Computing (NCBC) lab.

To avoid any potential bias and overfitting of the model training, we ensured the independent collection of training and test data using the *GeoSurvey*ⁱⁱⁱ mobile application for data collection. This approach helped in keeping the test set data independent and hidden from the model training. The accuracy of the models reported in the study is for the independent test set. Furthermore, during the training of the neural network training, we adopted the "dropout" strategy in which some of the neurons in the hidden layers are dropped out (deactivated) at random. The deactivated neurons neither participate in the forward pass nor get weight updates during the backpropagation. The dropout strategy effectively implies that distinct neurons were disregarded at every training iteration, and it proves to be an effective approach to overcoming the potential overfitting of the model. Randomly generated points within the study area, recorded via GPS coordinates, were cross-checked against the classified map to validate the identification of mineralization zones. These results underscore the effectiveness of the proposed methodology in leveraging deep learning and machine learning techniques for accurate mineral zone delineation and mapping within the study area.

5 | Conclusion and Future Work

The successful implementation of the hybrid CNN-SVM model for mineral deposit mapping presents exciting opportunities for extending this research to other valuable minerals found across different regions of the country. Future efforts will focus on leveraging the combined power of deep neural networks and machine learning algorithms to enhance accuracy and efficiency in mapping minerals such as gypsum, granite, soapstone, coal, iron, and copper. Expanding the scope of this study will involve adapting the hybrid model to accommodate different sensors and datasets. Specifically, we plan to explore the application of similar models with alternative sensor technologies, evaluating their effectiveness in diverse geological settings. Furthermore, future research will investigate the integration of ensemble models and transfer learning techniques to further optimize mineral mapping processes. Ensemble approaches, combining multiple models for improved prediction accuracy, and transfer learning, leveraging pre-trained models for enhanced performance in specific tasks, hold promise for advancing the capabilities

of remote sensing data analysis. We are extending the experimentation phase toward the performance evaluation of ensemble approaches like bagging and boosting on the same dataset and intend to compose a separate comprehensive research article on their outcomes which illustrates complete classification reports and a comparative analysis discussion. We intend to conduct similar experiments on close-range remote sensing data acquired through LiDAR (Light Detection and Ranging) and assess the mapping capabilities of various hybrid models while benefiting from the high-resolution spatial information provided by LiDAR. Our future work will also assess newer ensemble learning methods and transfer learning approaches to enhance accuracy while obtaining scalability and robustness of mineral explorations and mapping processes.

Author Contributions

Nazir Jan: conceptualization, methodology, software, investigation, writing – original draft. **Nasru Minallah:** conceptualization, resources, supervision. **Madiha Sher:** software, data curation, writing – original draft. **Muhammad Wasim:** methodology, investigation, writing – original draft. **Shahid Khan:** validation, formal analysis, visualization. **Amal Al-Rasheed:** writing – review and editing, funding acquisition. **Hazrat Ali:** validation, formal analysis, writing – review and editing.

Conflicts of Interest

The authors declare no conflicts of interest.

Data Availability Statement

The data that support the findings of this study are available from the corresponding author upon reasonable request.

Endnotes

ⁱ <https://portal.kpminerals.gov.pk>.

ⁱⁱ <https://earthexplorer.usgs.gov/>.

ⁱⁱⁱ <https://geosurveyapp.com/map/v2>.

References

1. İ. Henden, "Lineaments Map of Turkey From Landsat Imagery and Selecting Target Areas for Mineral Exploration, Relationship of Regional Lineaments to Earthquake Epicenters, Mineral Waters and Hot Springs," *Bulletin of the Mineral Research and Exploration* 1980, no. 95 (2023): 5.
2. J. Lubang, H. Liu, and R. Chen, "Combined Application of Hydrogeological and Geoelectrical Study in Groundwater Exploration in Karst-Granite Areas, Jiangxi Province," *Water* 15, no. 5 (2023): 865.
3. Y. Ghorbani, S. E. Zhang, G. T. Nwaila, et al., "Dry Laboratories–Mapping the Required Instrumentation and Infrastructure for Online Monitoring, Analysis, and Characterization in the Mineral Industry," *Minerals Engineering* 191 (2023): 107971.
4. Y. Ghorbani, G. T. Nwaila, S. E. Zhang, et al., "Moving Towards Deep Underground Mineral Resources: Drivers, Challenges and Potential Solutions," *Resources Policy* 80 (2023): 103222.
5. S. Wang, K. Guan, C. Zhang, et al., "Cross-Scale Sensing of Field-Level Crop Residue Cover: Integrating Field Photos, Airborne Hyperspectral Imaging, and Satellite Data," *Remote Sensing of Environment* 285 (2023): 113366.
6. S. A. Mohamed, M. M. Metwaly, M. R. Metwalli, M. A. AbdelRahman, and N. Badreldin, "Integrating Active and Passive Remote Sensing

- Data for Mapping Soil Salinity Using Machine Learning and Feature Selection Approaches in Arid Regions,” *Remote Sensing* 15, no. 7 (2023): 1751.
7. N. Jan, N. Minallah, M. Sher, J. Frnda, and J. Nedoma, “Deep Learning Based Minerals’ Recognition and Mapping Using Sentinel-2 Imagery,” *Research Square* (2023).
8. P. Kumari, S. Soor, A. Shetty, and S. G. Koolagudi, “Mineral Classification on Martian Surface Using CRISM Hyperspectral Data: A Survey,” *Journal of Applied Remote Sensing* 17, no. 4 (2023): 041501.
9. R. Oymatov, Z. Mamatkulov, R. Maksudov, et al., “Improving the Methods of Agricultural Mapping Using Remote Sensing Data,” *E3S Web of Conferences* 386 (2023): 04008.
10. C. A. D. Tsiakos and C. Chalkias, “Use of Machine Learning and Remote Sensing Techniques for Shoreline Monitoring: A Review of Recent Literature,” *Applied Sciences* 13, no. 5 (2023): 3268.
11. F. Nininahazwe, J. Théau, G. Marc Antoine, and M. Varin, “Mapping Invasive Alien Plant Species With Very High Spatial Resolution and Multi-Date Satellite Imagery Using Object-Based and Machine Learning Techniques: A Comparative Study,” *GIScience & Remote Sensing* 60, no. 1 (2023): 2190203.
12. A. R. Pathare and A. S. Joshi, *Dimensionality Reduction of Multivariate Images Using the Linear & Nonlinear Approach* (Dehradun, India: IEEE, 2023), 234–237.
13. B. Bai, Y. Tan, G. Donchyts, et al., “Naive Bayes Classification-Based Surface Water Gap-Filling From Partially Contaminated Optical Remote Sensing Image,” *Journal of Hydrology* 616 (2023): 128791.
14. A. Tariq, J. Yan, A. S. Gagnon, M. Riaz Khan, and F. Mumtaz, “Mapping of Cropland, Cropping Patterns and Crop Types by Combining Optical Remote Sensing Images With Decision Tree Classifier and Random Forest,” *Geo-Spatial Information Science* 26, no. 3 (2023): 302–320.
15. A. Tariq, Y. Jiango, Q. Li, et al., “Modelling, Mapping and Monitoring of Forest Cover Changes, Using Support Vector Machine, Kernel Logistic Regression and Naive Bayes Tree Models With Optical Remote Sensing Data,” *Heliyon* 9, no. 2 (2023), <https://doi.org/10.1016/j.heliyon.2023.e13212>.
16. D. Wang, J. Peng, Q. Yu, Y. Chen, and H. Yu, “Support Vector Machine Algorithm for Automatically Identifying Depositional Microfacies Using Well Logs,” *Sustainability* 11, no. 7 (2019): 1919.
17. X. Lan, C. Zou, Z. Kang, and X. Wu, “Log Facies Identification in Carbonate Reservoirs Using Multiclass Semi-Supervised Learning Strategy,” *Fuel* 302 (2021): 121145.
18. B. M. Usmanov, L. S. Isakova, S. S. Mukharamova, L. G. Akhmetzyanova, and I. N. Kuritsin, “Automated Detection of Illegal Nonmetallic Minerals Mining Places According to Sentinel-2 Data,” *SPIE Remote Sensing* 11863 (2021): 379–391.
19. H. Shirmard, E. Farahbakhsh, E. Heidari, et al., “A Comparative Study of Convolutional Neural Networks and Conventional Machine Learning Models for Lithological Mapping Using Remote Sensing Data,” *Remote Sensing* 14, no. 4 (2022): 819.
20. D. R. P. Lima, D. Duarte, C. Nicholson, R. Slatt, and K. J. Marfurt, “Petrographic Microfacies Classification With Deep Convolutional Neural Networks,” *Computers and Geosciences* 142 (2020): 104481.
21. S. Li, J. Chen, and J. Xiang, “Applications of Deep Convolutional Neural Networks in Prospecting Prediction Based on Two-Dimensional Geological Big Data,” *Neural Computing and Applications* 32 (2020): 2037–2053.
22. A. Koeshidayatullah, M. Morsilli, D. J. Lehrmann, K. Al-Ramadan, and J. L. Payne, “Fully Automated Carbonate Petrography Using Deep Convolutional Neural Networks,” *Marine and Petroleum Geology* 122 (2020): 104687.
23. M. Azarafza, M. Azarafza, H. Akgün, P. M. Atkinson, and R. Derakhshani, “Deep Learning-Based Landslide Susceptibility Mapping,” *Scientific Reports* 11, no. 1 (2021): 24112.
24. X. Sang, L. Xue, X. Ran, X. Li, J. Liu, and Z. Liu, “Intelligent High-Resolution Geological Mapping Based on SLIC-CNN,” *ISPRS International Journal of Geo-Information* 9, no. 2 (2020): 99.
25. J. Huang, Z. Jiang, H. Zhang, and Y. Yao, “Ship Object Detection in Remote Sensing Images Using Convolutional Neural Networks,” *Journal of Beijing University of Aeronautics and Astronautics* 43, no. 9 (2017): 1841.
26. X. Sun, L. Liu, C. Li, J. Yin, J. Zhao, and W. Si, “Classification for Remote Sensing Data With Improved CNN-SVM Method,” *IEEE Access* 7 (2019): 164507–164516.
27. X. Han, Y. Zhong, L. Cao, and L. Zhang, “Pre-Trained Alexnet Architecture With Pyramid Pooling and Supervision for High Spatial Resolution Remote Sensing Image Scene Classification,” *Remote Sensing* 9, no. 8 (2017): 848.
28. K. Zhang, B. He, S. Li, and Y. Shao, “Complex Scene Classification of Remote Sensing Images Based on CNN,” *Remote Sensing of Land Resources* 30, no. 2 (2018): 49–55.
29. Z. Zhang, X. Mi, J. Yang, et al., “Remote Sensing Image Scene Classification in Hybrid Classical-Quantum Transferring CNN With Small Samples,” *Sensors* 23, no. 18 (2023): 8010.
30. Y. Yao, Z. Wang, and P. Zhou, “Privacy-Preserving and Energy Efficient Task Offloading for Collaborative Mobile Computing in IoT: An ADMM Approach,” *Computers & Security* 96 (2020): 101886.
31. Z. Wang, Z. Yang, I. Azimi, and A. M. Rahmani, “Differential private federated transfer learning for mental health monitoring in everyday settings: A case study on stress detection,” *arXiv preprint arXiv:2402.10862* (2024).
32. X. X. Zhu, D. Tuia, L. Mou, et al., “Deep Learning in Remote Sensing: A Comprehensive Review and List of Resources,” *IEEE Geoscience and Remote Sensing Magazine* 5, no. 4 (2017): 8–36.
33. E. Maggiori, Y. Tarabalka, G. Charpiat, and P. Alliez, “Convolutional Neural Networks for Large-Scale Remote-Sensing Image Classification,” *IEEE Transactions on Geoscience and Remote Sensing* 55, no. 2 (2016): 645–657.
34. A. Mohan, A. K. Singh, B. Kumar, and R. Dwivedi, “Review on Remote Sensing Methods for Landslide Detection Using Machine and Deep Learning,” *Transactions on Emerging Telecommunications Technologies* 32, no. 7 (2021): e3998.
35. M. I. Abdulraheem, W. Zhang, S. Li, A. J. Moshayedi, A. A. Farooque, and J. Hu, “Advancement of Remote Sensing for Soil Measurements and Applications: A Comprehensive Review,” *Sustainability* 15, no. 21 (2023): 15444.
36. G. U. Sikakwe, “Mineral Exploration Employing Drones, Contemporary Geological Satellite Remote Sensing and Geographical Information System (GIS) Procedures: A Review,” *Remote Sensing Applications: Society and Environment* 31 (2023): 100988.
37. J. Segarra, M. L. Buchaillet, J. L. Araus, and S. C. Kefauver, “Remote Sensing for Precision Agriculture: Sentinel-2 Improved Features and Applications,” *Agronomy* 10, no. 5 (2020): 641.
38. H. Alikhani, Z. Wang, A. Kanduri, P. Lilieberg, A. M. Rahmani, and N. Dutt, *SEAL: Sensing Efficient Active Learning on Wearables Through Context-Awareness* (Valencia, Spain: IEEE, 2024), 1–2.
39. T. Sun, H. Li, K. Wu, F. Chen, Z. Zhu, and Z. Hu, “Data-Driven Predictive Modelling of Mineral Prospectivity Using Machine Learning and Deep Learning Methods: A Case Study From Southern Jiangxi Province, China,” *Minerals* 10, no. 2 (2020): 102.
40. Z. Wang, N. Luo, and P. Zhou, “GuardHealth: Blockchain Empowered Secure Data Management and Graph Convolutional Network Enabled

- Anomaly Detection in Smart Healthcare,” *Journal of Parallel and Distributed Computing* 142 (2020): 1–12.
41. X. Yang, H. Liu, Z. Wang, and P. Gao, “Zebra: Deeply integrating system-level provenance search and tracking for efficient attack investigation,” *arXiv preprint arXiv:2211.05403* (2022).
42. W. Jiang, Y. Zhan, S. Xi, D. D. Huang, and J. Lu, “Compressive Sensing-Based 3-d Rain Field Tomographic Reconstruction Using Simulated Satellite Signals,” *IEEE Transactions on Geoscience and Remote Sensing* 60 (2021): 1–13.
43. B. Yang, X. Wang, Y. Xing, C. Cheng, W. Jiang, and Q. Feng, “Modality Fusion Vision Transformer for Hyperspectral and LiDAR Data Collaborative Classification,” *IEEE Journal of Selected Topics in Applied Earth Observations and Remote Sensing* 17 (2024): 17052–17065.
44. K. Itano and H. Sawada, “Revisiting the Geochemical Classification of Zircon Source Rocks Using a Machine Learning Approach,” *Mathematical Geoscience* 56 (2024): 1139–1160.
45. G. Mountrakis, J. Im, and C. Ogole, “Support Vector Machines in Remote Sensing: A Review,” *ISPRS Journal of Photogrammetry and Remote Sensing* 66, no. 3 (2011): 247–259.
46. A. Khan, A. Sohail, U. Zahoor, and A. S. Qureshi, “A Survey of the Recent Architectures of Deep Convolutional Neural Networks,” *Artificial Intelligence Review* 53 (2020): 5455–5516.
47. W. Rawat and Z. Wang, “Deep Convolutional Neural Networks for Image Classification: A Comprehensive Review,” *Neural Computation* 29, no. 9 (2017): 2352–2449.
48. O. Saliu, D. Curilla, M. Lennon, and A. Chung, *Lessons learned: Deep learning for mineral exploration* (Bogotá, Colombia: European Association of Geoscientists & Engineers, 2020), 1–1.
49. J. Zhang, “Multi-Source Remote Sensing Data Fusion: Status and Trends,” *International Journal of Image and Data Fusion* 1, no. 1 (2010): 5–24.
50. V. Rodriguez-Galiano, M. Sanchez-Castillo, M. Chica-Olmo, and M. Chica-Rivas, “Machine Learning Predictive Models for Mineral Prospectivity: An Evaluation of Neural Networks, Random Forest, Regression Trees and Support Vector Machines,” *Ore Geology Reviews* 71 (2015): 804–818.
51. F. Mohsen, H. Ali, N. El Hajj, and Z. Shah, “Artificial Intelligence-Based Methods for Fusion of Electronic Health Records and Imaging Data,” *Scientific Reports* 12, no. 1 (2022): 17981.
52. J. Wan and Y. Ma, “Multi-Scale Spectral-Spatial Remote Sensing Classification of Coral Reef Habitats Using CNN-SVM,” *Journal of Coastal Research* 102, no. SI (2020): 11–20.
53. S. Hajaj, A. El Harti, A. Jellouli, et al., “Evaluating the Performance of Machine Learning and Deep Learning Techniques to HyMap Imagery for Lithological Mapping in a Semi-Arid Region: Case Study From Western Anti-Atlas, Morocco,” *Minerals* 13, no. 6 (2023): 766.
54. M. A. El-Omairi and A. El Garouani, “A Review on Advancements in Lithological Mapping Utilizing Machine Learning Algorithms and Remote Sensing Data,” *Heliyon* 9 (2023): e20168.
55. M. Wasim, F. Al-Obeidat, A. Amin, H. Gul, and F. Moreira, “Enhancing Link Prediction Efficiency With Shortest Path and Structural Attributes,” *Intelligent Data Analysis* 28 (2024): 467–483.
56. A. Eskandari, M. Hosseini, and E. Nicotra, “Application of Satellite Remote Sensing, UAV-Geological Mapping, and Machine Learning Methods in the Exploration of Podiform Chromite Deposits,” *Minerals* 13, no. 2 (2023): 251.
57. S. Iqbal, D. Ali, and B. Khan, “Examining AI and Machine Learning’s Implications in Mineral Investigation,” *Exceed Journal of Biological and Computer Sciences* 1, no. 1 (2024): 1–22.
58. H. Bahrami, P. Esmaeili, S. Homayouni, A. B. Pour, K. Chokmani, and A. Bahroudi, “Machine Learning-Based Lithological Mapping From ASTER Remote-Sensing Imagery,” *Minerals* 14, no. 2 (2024): 202.
59. H. Shirmard, E. Farahbakhsh, R. D. Müller, and R. Chandra, “A Review of Machine Learning in Processing Remote Sensing Data for Mineral Exploration,” *Remote Sensing of Environment* 268 (2022): 112750.
60. N. Jan, N. Minallah, N. Gohar, et al., “Granite Exposure Mapping Through Sentinel-2 Visible and Short Wave Infrared Bands,” *Radio Science* 59, no. 2 (2024): 1–12.
61. L. Yao, X. Wang, J. Zhang, X. Yu, S. Zhang, and Q. Li, “Prediction of Sea Surface Chlorophyll-a Concentrations Based on Deep Learning and Time-Series Remote Sensing Data,” *Remote Sensing* 15, no. 18 (2023): 4486.
62. Y. Xu, Z. Wu, and Z. Wei, “Spectral–Spatial Classification of Hyperspectral Image Based on Low-Rank Decomposition,” *IEEE Journal of Selected Topics in Applied Earth Observations and Remote Sensing* 8, no. 6 (2015): 2370–2380.
63. H. Moradpour, G. Rostami Paydar, A. B. Pour, et al., “Landsat-7 and ASTER Remote Sensing Satellite Imagery for Identification of Iron Skarn Mineralization in Metamorphic Regions,” *Geocarto International* 37, no. 7 (2022): 1971–1998.
64. S. Manfreda and E. B. Dor, “Remote Sensing of the Environment Using Unmanned Aerial Systems. Unmanned Aerial Systems for Monitoring Soil, Vegetation, and Riverine Environments,” in *Unmanned Aerial Systems for Monitoring Soil, Vegetation, and Riverine Environments*, eds. S. Manfreda and E. Ben Dor (Amsterdam, Netherlands: Elsevier, 2023), 3–36.

Appendix A

A.1 | Hardware Specifications

The model developed in the study were run on a Windows-based computer with Intel Xeon Processor 64GB memory, equipped with an NVIDIA RTX 16000 GPU. The model training took 1 h and 15 min to complete the preset epochs. It took 25 min on the test set data to generate the given outcomes.

A.2 | Image Processing

The image processing stage is essential for enhancing image quality and removing undesired and redundant bands while preserving relevant features such as lines and edges in the picture data. During this stage, techniques like Principal Components Analysis (PCA) and Minimum Noise Fraction (MNF) are commonly employed to optimize remote sensing (RS) data. MNF offers distinct advantages over PCA due to its multi-fold operations on RS data, which effectively reduce spectral dimensions while mitigating noise and eliminating tainted bands. This process is crucial as hyperspectral data often contains noise and unwanted bands, particularly from water vapor and air pollution, resulting in poor band quality. Regular cleaning of such bands is necessary to enhance data quality. In the study, multispectral data were utilized, and careful selection of appropriate bands was conducted for layer stacking, as outlined in Table A1. This selection process ensures that only relevant and high-quality bands are retained for subsequent analysis and interpretation.

A.3 | Alternative Sources of Data

We have used publicly accessible Sentinel-2 remote sensing data, which can be obtained for every region included in the study from several sources like USGS. As alternatives, comparable data with similar bands (VNIR, SWIR, and TIR) can also be obtained from other multispectral

TABLE A1 | The selected minerals bands for layer stacking.

Sentinel-2 Satellite's spectral, spatial, and radiometric resolution details				
Index	Spectral bands	Wavelengths	Resolution	Radiometric resolution
1	Ultra-Blue Aerosol Band)	443 nm	60 m	12 bits
2	Blue	490 nm	10 m	—
3	Green	560 nm	—	—
4	Red	665 nm	—	—
5–7	Visible Near-Infrared (VNIR)	705–783 nm	20 m	—
8	Visible Near-Infrared (VNIR)	842 nm	10 m	—
8a	Visible Near-Infrared (VNIR)	865 nm	20 m	—
9	Shortwave-Infrared (SWIR)	940 nm	60 m	—
10	Shortwave-Infrared (SWIR)	1375 nm	—	—
11	Shortwave-Infrared (SWIR)	1610 nm	20 m	—
12	Shortwave-Infrared (SWIR)	2190 nm	—	—

sensors such as Landsat 9, Landsat 8, Landsat 7, and ASTER for the mapping of minerals [63]. In addition to distant space-borne satellites, alternative platforms and approaches for data acquisition include UAVs (also known as drones), piloted aircraft, balloons, ground-based radars, LiDAR, and field spectrometers [64].